Pulsed ENDOR Study of Water Coordination to Gd^{3+} Complexes in Orientationally Disordered Systems

Andrei V. Astashkin* and Arnold M. Raitsimring*

Department of Chemistry, University of Arizona, Tucson, Arizona 85721

Peter Caravan

EPIX Medical, Incorporated, 71 Rogers Street, Cambridge, Massachusetts 02142

Received: June 20, 2003; In Final Form: December 8, 2003

In orientationally disordered systems, the ENDOR (electron−nuclear double resonance) spectra of high-spin ions having weak crystal field interaction (cfi) contain nuclear transition lines (often overlapped) that belong to several different electron spin manifolds, and the transition lines for each manifold are distorted by the effect of the cfi. In this work, we have shown that, although the latter distortions can be quite considerable in a general case, the statistical distributions of the cfi parameters and orientations of the cfi axes in glassy samples result in ENDOR line shapes similar to the usual powder pattern determined by the hyperfine interaction only, which greatly simplifies their analysis. We have also shown that the two-dimensional Mims ENDOR technique can be used to disentangle the nuclear transitions that belong to different electron spin manifolds. The results of the analysis were applied to study the Gd^{3+} aquo complex and the Gd^{3+}-based MRI contrast agent GdHPDO3A in frozen glassy water/methanol solutions. The average distance between Gd and protons of the water ligands was found to be about 3.1 Å for both complexes.

1. Introduction

Gadolinium complexes are used clinically as diagnostic contrast agents for magnetic resonance imaging (MRI) in medicine. They function by catalytically enhancing the magnetic relaxation rates of water protons. The contrast agents typically contain one inner-sphere water molecule that is in fast exchange with bulk solvent. In practical applications, MRI agents are characterized by relaxivity, a bulk parameter that shows the extent to which the ion can change the relaxation rate of solvent protons. Increased relaxivity allows the contrast agent to be administered at a lower dose or enables the imaging of low-concentration targets and is the focus of extensive academic and industrial research.[1−19]

Relaxivity is a complex function of numerous parameters, such as the ion relaxation times (that depend on the crystal field interaction (cfi) of the ion), the number of water molecules in the inner and outer coordination spheres, the average time these water molecules spend in a coordinated state, the ion−hydrogen distances for coordinated water molecules, the rotational diffusion of the complex, and so forth. Reported relaxivity values measured by ^{1}H nuclear magnetic resonance (NMR) in standard conditions (at the frequency of 20 MHz and the temperature of 25 °C) for Gd^{3+} complexes range from about 2 to 150 mM^{-1} s^{-1}.[1,2] These differences in the relaxivity can often be rationalized by considering the number of coordinated water molecules and the rotational diffusion time of the complex. For example, the high relaxivity value of 148 for a Gd^{3+} ion bound to the protein glutamine synthetase is explained by the combination of a relatively large number of water ligands (four) and very long rotational diffusion time, whereas the low molecular weight complex GdBPO4A with the relaxivity value of only about 1.7 has a relatively short correlation time and does not have inner-sphere water ligands.[4]

On the other hand, complexes of similar structure that should have similar correlation times and the same number of water ligands exhibit about a 3-fold variation in relaxivities, which was explained by some workers by a possible variation of the Gd−H distance, R_{GdH}, from complex to complex. The overall range of the reported R_{GdH} values is from 2.5 to 3.3 Å,[20−22] with the values of 2.90−3.13 Å being more common.[1,10,11]

Because the relaxivity is proportional to $1/R_{GdH}^6$, large variations in relaxivity could, in principle, be conveniently explained by moderate changes of R_{GdH}. The range of the reported distances, however, seems to be too large because the distances between the Gd ion and the oxygen of the coordinated water determined by X-ray crystallography for different complexes are all very similar, 2.41−2.56 Å.[1] The clarification of this discrepancy necessitates further effort aimed at determining R_{GdH} with possibly high accuracy, which would allow one to factor out the $1/R_{GdH}^6$ dependence from the relaxivity and provide for a better understanding of other parameters that could, possibly, be manipulated to enhance the relaxivity of contrast agents. The $1/R_{GdH}^6$ dependence of the relaxivity implies that the accuracy of distance measurements has to be rather high. With a 3-fold variation of the relaxivity for the contrast agents that have similar size and the same number of water ligands,[1] it is clear that the accuracy should be about 1 order of magnitude better than 20% ($1.2 \approx 3^{1/6}$), that is, about 2%.

The $1/R_{GdH}^6$ factor in the relaxivity originates from the anisotropic hyperfine interaction (hfi) between the electron and nuclear spins. Therefore, the most appropriate techniques to deal with this factor would be those of magnetic resonance because they allow one to determine the anisotropic hfi directly. The

* Authors to whom correspondence should be addressed. (A.V.A.) Phone: (520) 621-9968. Fax: (520) 621-8407. E-mail: andrei@u.arizona.edu. (A.M.R.) Phone: (520) 621-9968. Fax: (520) 621-8407. E-mail: arnold@u.arizona.edu.

10.1021/jp0307811 CCC: $27.50
Published on Web 02/20/2004

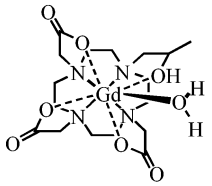

Figure 1. The contrast agent Gd^{3+}HPDO3A.

isotropic hfi of the ligand protons (that, in principle, also contributes to the relaxivity) can also be determined, but it is expected to be negligibly small because the π-bonding interactions between the ligand molecular orbitals and f-orbitals of Gd^{3+} are weak. The spin density transferred from Gd to the direct ligands (in the case of a H_2O molecule, the oxygen atom) is expected to be no more than 0.3%.[6−8] Therefore, the proton anisotropic hfi is sufficiently accurately described by the point dipole model, and the distance R_{GdH} can be readily evaluated.

In a few publications where magnetic resonance methods, electron spin−echo envelope modulation (ESEEM), and electron−nuclear double resonance (ENDOR) spectroscopies were employed, quite different values of R_{GdH} were obtained. An application of continuous wave (CW) ENDOR to Gd-doped lanthanum ethyl sulfate[23] and lanthanum nicotinate[24] single crystals resulted in estimates of R_{GdH} in the range from about 3 to 3.2 Å, whereas in glassy water/methanol solution the values of R_{GdH} for various complexes were estimated to be in the range of 2.5−3.1 Å.[21] In the only ESEEM work[22] on contrast agents the Gd−H distances were found to be about 2.7 Å.

The distances found for glassy samples are, on average, significantly shorter than those in single crystals. This could imply a fundamental change in water coordination when structural constrains imposed by crystal lattice were removed. On the other hand, the experimental ESEEM traces[22] and ENDOR spectra[21] for Gd^{3+} complexes in glassy solutions were exclusively attributed to the nuclear spin transitions within the electron spin manifolds with $m_S = \pm^1/_2$, which could result in inaccurate hfi parameters and Gd−H distances. Resolving this issue is necessary not only in relation to the relaxivity but also for understanding if the structures of the Gd complexes in glassy and crystalline systems are actually different.

In this work we used pulsed ENDOR to study glassy water/methanol solutions of Gd^{3+} and one of the commercial contrast agents, Gd^{3+}HPDO3A (Prohance, Bracco Diagnostics, Figure 1). The theoretical results of our previous work[25] were used to analyze the spectra. The Gd−H distances we found from our experiments and analysis are similar to those obtained earlier in single-crystal studies,[23,24] the distances reported for glassy samples elsewhere[21,22] thus being significantly underestimated. The analysis performed in this work shows also that some of the problems related to the high-spin nature of Gd^{3+} ion can be alleviated, and the hfi parameters be obtained with a good accuracy, if a two-dimensional (2D) pulsed ENDOR technique due to Mims[26,27] is used. Such an approach can be employed for investigation of the immediate nuclear environment of any high-spin ion characterized by weak cfi.

2. Experimental Section

The experiments were performed with frozen 3 mM solutions of Gd complexes ($GdCl_3$ and GdHPDO3A) in 1:1 (v/v) H_2O/CD_3OH (methanol added for glassification). With this methanol concentration, about one-third of potential ligands to the Gd^{3+} ions were methanol molecules. Keeping this in mind, we will refer to the ligands simply as water ligands for brevity and because only about one-fifth of the protons of coordinated $OH_{(2)}$ groups belong to methanol.

Mims ENDOR[26] measurements were performed on a home-built pulsed EPR (electron paramagnetic resonance) spectrometer operating in the microwave (mw) frequency range from 8 to 18 GHz (X- and K_u-bands) and equipped with a helium-flow cryostat (Oxford CF935) and a pulsed ENDOR accessory. To provide the smallest possible ratio of cfi to the electron−Zeeman interaction, the measurements were performed in the mw K_u-band, at the mw frequencies of about 14.4 and 17.1 GHz. The cylindrical dielectric ENDOR resonator was similar in design to that described earlier[28] but had smaller overall dimensions and, consequently, higher resonance frequencies. The radio frequency (RF) amplifier AR-250L (Amplifier Research) provided a nominal output power of about 1 kW in the pulsed mode. The measurement temperature was 4.2 K (liquid He).

Before the Fourier transform was performed on the experimental 2D Mims ENDOR traces, these traces were normalized by stimulated electron spin−echo (ESE) decays recorded without the RF. This treatment prevented the ESEEM spectral lines from appearing in the 2D spectra and was justified in this case because the stimulated ESEEM was contributed by weakly coupled ^1H and ^2D and consisted of oscillations with the Zeeman frequencies of these nuclei. The experimental 2D Mims ENDOR spectra were overwhelmingly dominated by the line due to distant matrix protons. Therefore, for presentation purposes, in order to make other spectral features more visible, the 2D spectra were multiplied by $1 - \exp[-2(\nu_{RF} - \nu_H)^2/(\delta\nu)^2]$, where ν_{RF} is the radio frequency, ν_H is the Zeeman frequency of protons, and $\delta\nu = 1$ MHz. Such a multiplication suppressed the peak due to distant matrix protons within the frequency range of about 1 MHz around $\nu_{RF} = \nu_H$.

3. Theoretical Background

3.1. Effect of Weak cfi on Nuclear Transition Frequencies. Recently[25] we performed a theoretical analysis of ESEEM for high-spin ($S > {}^1/_2$) ions characterized by weak cfi. We showed that, in addition to a well-known lifting of degeneracy of EPR transitions, weak cfi is also able to significantly distort the spectra of nuclear transitions compared to those without the cfi. These distortions are caused by departures of electron spin quantization axes (different for different electron spin manifolds) from the direction of the external magnetic field $\mathbf{B_0}$. As an application of the theory we mainly considered ESEEM of the Mn^{2+} aquo ion that has $S = {}^5/_2$ and the axial crystal field parameter $D/g\beta \sim -200$ G (g is the g-factor and β is the Bohr magneton). Model simulations for Mn^{2+} aquo ion in an orientationally disordered matrix have shown that distortions of X-band ENDOR spectra by the cfi are not very significant.[25] In this work we are concerned with ENDOR of complexes of Gd^{3+} ions that have a higher electron spin ($S = {}^7/_2$) and a stronger cfi. We found that the crystal field distortions of the ENDOR spectra of these complexes are considerably stronger than those for aquo Mn^{2+} and have to be properly accounted for in a practical analysis. Because the theory developed in our previous work[25] is fully applicable to ENDOR, we reiterate here the expressions relevant to the interpretation of ENDOR spectra.

The paramagnetic complex will be characterized by the D and E parameters that account for the quadrupolar part of the

cfi. The fine structure spin Hamiltonian in the laboratory coordinate frame *XYZ* is thus[29]

$$H_{\mathrm{FS}} = g\beta\beta_o S_Z + D\left(S_{Z_c}^2 - \frac{1}{3}S(S+1)\right) + E(S_{X_c}^2 - S_{Y_c}^2) \quad (1)$$

where X_c, Y_c, and Z_c are the principal axes of the cfi. The cfi parameters D and E are considered to be small: $g\beta B_o \gg D, E$.

With weak cfi, the eigenfunctions of Hamiltonian 1 are still close to the original basis functions $|\pm^1/_2\rangle$, $|\pm^3/_2\rangle$, $|\pm^5/_2\rangle$, and $|\pm^7/_2\rangle$, and the electron spin projections $m_Z = \langle S_Z\rangle$ for these states, to the first order in $(D,E)/g\beta B_o$, are equal to $\pm^1/_2$, $\pm^3/_2$, $\pm^5/_2$, and $\pm^7/_2$, respectively. Because of slight admixture of other states into each state with given m_Z, however, the electron spin projections on laboratory axes X and Y are generally nonzero and equal to (neglecting terms quadratic in $(D,E)/g\beta B_o$)[25]

$$m_X \approx \frac{Dc_{\theta_c}s_{\theta_c}c_{\varphi_c} - E(c_{\theta_c}s_{\theta_c}c_{\varphi_c}c_{2\psi_c} - s_{\theta_c}s_{\varphi_c}s_{2\psi_c})}{g\beta\beta_o}(3m_z^2 - S(S+1))$$

$$m_Y \approx \frac{Dc_{\theta_c}s_{\theta_c}c_{\varphi_c} - E(c_{\theta_c}s_{\theta_c}s_{\varphi_c}c_{2\psi_c} + s_{\theta_c}c_{\varphi_c}s_{2\psi_c})}{g\beta\beta_o}(3m_z^2 - S(S+1)) \quad (2)$$

where "*s*" and "*c*" with subscripts φ_c, θ_c, and ψ_c ($2\psi_c$) denote sines and cosines of the Euler angles φ_c, θ_c, and ψ_c relating the coordinate systems *XYZ* and $X_cY_cZ_c$. They are the angles of three consecutive rotations: (1) around Z_c by φ_c, (2) around the newly obtained Y_c by θ_c, and (3) around the newly obtained Z_c by ψ_c. The situation with all the angles equal to zero corresponds to the orientation of $X//X_c$, $Y//Y_c$, and $Z//Z_c$.

The Hamiltonian for matrix and ligand nuclei of spin $I = {}^1/_2$ (e.g., protons) that includes their hf and Zeeman interactions is

$$H_{\mathrm{HF}} = -\nu_I I_Z + a_{\mathrm{iso}}\mathbf{SI} + \mathbf{STI} \quad (3)$$

where $\nu_I = g_n\beta_n B_o$ (g_n is the nuclear g-factor and β_n is the nuclear magneton), a_{iso} is the isotropic hfi constant, and $\mathbf{T}$ is the anisotropic hfi tensor.

We consider here the ligand hfi to be weak compared with the electronic Zeeman and cf interactions: $a_{\mathrm{iso}}, T_{ij} \ll g\beta B_o, D, E$. The weak ligand hfi practically does not mix electron spin functions, and the various terms of Hamiltonian 3 for a given spin state can be rearranged according to nuclear spin projections

$$H_{\mathrm{HF}} = (-\nu_I + m_Z a_Z)I_Z + m_Z A_X I_X + m_Z A_Y I_Y \quad (4)$$

where

$$A_Z = a_{\mathrm{iso}} + T_{ZZ} + T_{XZ}\frac{m_X}{m_Z} + T_{YZ}\frac{m_Y}{m_Z}$$

$$A_X = T_{ZX} + (a_{\mathrm{iso}} + T_{XX})\frac{m_X}{m_Z} + T_{YX}\frac{m_Y}{m_Z} \quad (5)$$

$$A_Y = T_{ZY} + T_{XY}\frac{m_X}{m_Z} + (a_{\mathrm{iso}} + T_{YY})\frac{m_Y}{m_Z}$$

and the electron spin operators are substituted by their average values, $\langle S_Z\rangle \approx m_Z$, $\langle S_X\rangle = m_X$, and $\langle S_Y\rangle = m_Y$. The nuclear transition frequency for an electron spin manifold with a given m_Z is given by

$$\upsilon_{m_Z} = \sqrt{m_Z^2B^2 + (\nu_I - m_Z A_Z)^2} \quad (6)$$

where $B = \sqrt{A_X{}^2 + A_Y{}^2}$.

One can see that the cfi contributes to the effective hfi values A_k (see eqs 5 and 2), and therefore the nuclear transition frequencies and the shape of ENDOR spectra will depend on the magnitude of the cfi parameters and on the orientation of $\mathbf{B_o}$ and the hfi tensor $\mathbf{T}$ in the cfi reference frame. The effect of the cfi can be immediately appreciated if we assume $\nu_I \gg m_Z A_Z$ (the so-called weak hfi limit) and expand eq 6 retaining only the terms linear in hfi

$$\nu_{m_Z} \approx \nu_I - (a_{\mathrm{iso}} + T_{ZZ})m_Z - T_{XZ}m_X - T_{YZ}m_Y \approx \nu_I - (a_{\mathrm{iso}} + T_{ZZ})m_Z - \frac{Dc_{\theta_C}s_{\theta_C}}{g\beta B_o}(3m_Z^2 - S(S+1))(c_{\varphi_C}T_{XZ} + s_{\varphi_C}T_{YZ}) \quad (7)$$

where we have also assumed for simplicity $E = 0$ and substituted explicit expressions for m_X and m_Y (eq 2). The first two terms in this expression give the usual nuclear transition frequency (accurate to first order in hfi) that would be observed for $D = 0$. The third term gives the correction to the nuclear transition frequency due to the cfi.

It follows from eq 7 that the frequency deviations from the $D = 0$ case disappear if $\mathbf{B_o}$ is aligned parallel to any of the principal axes of the hfi tensor because in such orientations all nondiagonal tensor elements T_{ij} are equal to zero (the nonzero components T_{XX} and T_{YY} contributing to B in the original eq 6 will result in second-order frequency shifts that are small in the weak hfi case). In addition, when each of the laboratory frame and the crystal field frame axes coincide, the electron spin projections m_X and m_Y become zero, and the effect of the cfi on the nuclear transition frequencies again disappears.

We can cast eq 7 in terms of the deviation of ν_{m_Z} from the nuclear Zeeman frequency, $\Delta\nu_{m_Z} = \nu_{m_Z} - \nu_I$

$$\frac{\Delta\nu_{m_Z}}{m_Z} \approx a_{\mathrm{iso}} + T_{ZZ} + \frac{Dc_{\theta_C}s_{\theta_C}}{g\beta B_o}\cdot\frac{(3m_Z^2 - S(S+1))}{m_Z}(c_{\varphi_C}T_{XZ} + s_{\varphi_C}T_{YZ}) \quad (8)$$

The cfi term in this expression is proportional to the factor $(3m_Z^2 - S(S+1))/m_Z$ that, with $S = {}^7/_2$, equals to ∓ 30, ∓ 6, ± 1.2, and ± 6 for the electron spin manifolds with $m_Z = \pm^1/_2$, $\pm^3/_2$, $\pm^5/_2$, and $\pm^7/_2$, respectively. One can see that the relative deviations of nuclear transition frequencies from those determined by hfi only are the largest for the electron spin manifolds with $m_Z = \pm^1/_2$. In fact, even if the condition of weak cfi is satisfied very well (e.g., $D/g\beta B_o \sim 0.03$), the cfi term in eq 8 may still be comparable with the hfi terms at some of the relative orientations of $\mathbf{B_o}$ and hfi and cfi tensors. For $m_Z = \pm^3/_2$ and $\pm^7/_2$ the relative contribution of the cfi term becomes one-fifth of that of $m_Z = \pm^1/_2$, and the minimal contribution is reached for $m_Z = \pm^5/_2$.

It follows from these considerations that if one is primarily concerned with accurate determination of the hfi, then the best nuclear spin transitions to study are those within the $\pm^5/_2$

electron spin manifolds. To do so, one must overcome certain experimental difficulties related to the fact that at insufficiently low temperatures all electron spin manifolds will be populated, and the respective nuclear transition lines will all contribute to the ENDOR spectra. The lines from $m_Z = \pm 5/2$ manifolds will then be difficult to trace because, in a disordered system, their width will be greater, and the intensity smaller, than those of the lines from the manifolds with $m_Z = \pm 3/2$ and $m_Z = \pm 1/2$. A practical solution to this problem is to increase the mw frequency, ν_{mw}, and decrease the temperature in order to selectively populate the electron spin manifold with $m_Z = -7/2$. For example, a combination of $\nu_{mw} \geq 90$ GHz (W-band or higher; typical B_o values for $g = 2$ are about 30 kG or greater) and $T \leq 2$ K will provide the population of the electron spin energy level with $m_Z = -7/2$ at least 1 order of magnitude greater than that of the next level, with $m_Z = -5/2$. Although, to our knowledge, W-band (or D-band, ~140 GHz) ENDOR was never used for investigations of Gd complexes, it could be the right choice for such studies, especially since the equipment for high-frequency pulsed EPR/ENDOR measurements is becoming increasingly common.[30−32]

Despite the strongest cfi effect on the nuclear transition frequencies within the $m_Z = \pm 1/2$ electron spin manifolds, using the ENDOR spectra of these transitions may still represent an attractive alternative to the high-frequency/low-temperature approach described above. In orientationally disordered systems the lines of nuclear transitions at $m_Z = \pm 1/2$ are several times narrower than those at other m_Z, providing the largest ENDOR effect. In addition, the EPR line that corresponds to the transition between $m_Z = 1/2$ and $m_Z = -1/2$ is much narrower than the lines of other EPR transitions because it is only broadened by the second-order cfi effects. This allows one to use moderate temperatures (~4 K) and moderate mw frequencies/magnetic fields and to benefit in these conditions from the highest relative intensity of this EPR line. Therefore, this approach is the most convenient one in terms of *detection and acquisition* of the ENDOR spectra. To be fully usable, however, it should be supplemented by the analysis of the spectra that properly accounts for the cfi effects.

In the following section we analyze the effect of weak cfi on the ^{1}H ENDOR spectra at $m_Z = \pm 1/2$ using numerical calculations. We show that the distribution of the cfi parameters results in a great simplification of these spectra and their subsequent interpretation. The results of this background work are then applied to the analysis of experimental spectra obtained at the K_u mw band.

3.2. Numerical Simulations of ENDOR Spectra. In the simulations we used proton hfi parameters close to those obtained in single-crystal studies;[23,24] namely, the isotropic hfi constant a_{iso} in our simulations was assumed to be equal to zero. The anisotropic hfi tensor was assumed to be axial, with the coupling constant $T_\perp \sim -3$ MHz. The cfi tensor was also assumed to be axial. The magnetic field $B_o = 6100$ G was close to the one actually used in some of our experiments described below. The proton Zeeman frequency is denoted ν_H, and it corresponds to a general nuclear Zeeman frequency, ν_I, used in theoretical expressions.

Figure 2a shows the ENDOR spectrum in an orientationally disordered system calculated for $D = 0$. This spectrum is similar to what one expects to observe for an $S = 1/2$ system in the case of a purely dipolar coupling between the electron and nuclear spins. The peaks in this spectrum are separated by the hfi constant $A_\perp = T_\perp$ (realized when the hfi axis is perpendicular to $\mathbf{B_o}$), whereas the shoulders are separated by the hfi constant

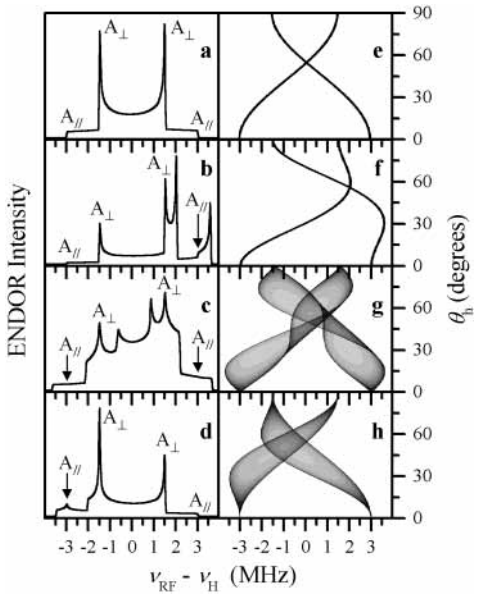

Figure 2. ENDOR calculations for an orientationally disordered system having a fixed angle θ_{hc} between the main principal axes of axial hfi and cfi tensors; $S = 7/2$, $I = 1/2$ (proton), $-1/2 \leftrightarrow 1/2$ electron spin transition. Common parameters are $a_{iso} = 0$ MHz, $T_\perp = -3$ MHz, $B_o = 6100$ G. Panels a−d show CW ENDOR spectra, whereas panels e−h show the dependences of nuclear transition frequencies on the angle θ_h between the hfi axis and $\mathbf{B_o}$. In panels a and e $D/g\beta = 0$. In all other panels $D/g\beta = 400$ G. The angle θ_{hc} is 0° (panels b,f), 45° (panels c,g), and 90° (panels d,h). Labels "$A_{||}$" and "$A_\perp$" mark the features corresponding to, respectively, parallel and perpendicular orientations of the hfi axis relative to $\mathbf{B_o}$.

$A_{||} = -2T_\perp$ (realized when the hfi axis is parallel to $\mathbf{B_o}$). Panels b−d of Figure 2 show the ENDOR spectra calculated for $D/g\beta = 400$ G and different angles θ_{hc} between the main axis of the hfi tensor and axis Z_c of the cfi tensor. The spectral positions corresponding to $A_{||}$ and $A_\perp$ are marked in all of these spectra as "$A_{||}$" and "$A_\perp$", respectively.

One can see that the spectra in panels b−d of Figure 2 are very different from that in Figure 2a. They are more broad, asymmetric, and show several additional singularities. The origin of all these features is easily understood from panels e−h of Figure 2 that show how the frequencies ν_{m_Z} depend on the angle θ_h between $\mathbf{B_o}$ and the main hfi axis. With $\theta_{hc} = 0$ (Z_c is parallel to the hfi axis, see Figure 2f) each orientation of the hfi axis corresponds to a unique orientation of Z_c, and therefore the dependence of each nuclear transition frequency on θ_h is represented by a single line. With $\theta_{hc} \neq 0$, however, for each θ_h there is a distribution of angles θ_c between the cfi axis Z_c and $\mathbf{B_o}$, and therefore, the dependence of each nuclear transition frequency on θ_h is represented by a strip of varying width (see panels g and h of Figure 2, calculated for $\theta_{hc} = 45°$ and 90°, respectively).

In the case of $D = 0$ the frequencies ν_{m_Z} are confined within the limits corresponding to the angles $\theta_h = 0°$ and 90°. With $D \neq 0$, however, the frequencies corresponding to intermediate θ_h values may become greater or smaller than the limiting frequency values at $D = 0$, which leads to the asymmetric spectral broadening. Nuclear transition frequencies at $\theta_h = 0°$ and 90° remain virtually unaffected, as mentioned above. The numerous singularities seen in the ENDOR spectra of panels b−d of Figure 2, as those in Figure 2a, correspond to all possible situations when $d\nu_{m_Z}/d\theta_h = 0$. Clearly, if such spectra were observed in experiment, it would be impossible to determine, without extensive numerical simulations, which set of singularities belongs to $A_{||}$ and $A_\perp$.

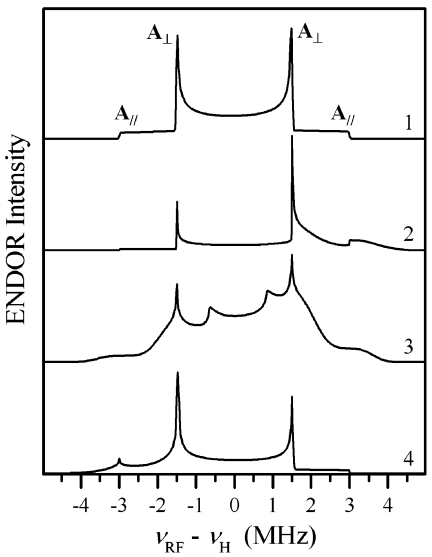

Figure 3. Calculated CW ENDOR spectra for an orientationally disordered system with $S = {}^7/_2$, $I = {}^1/_2$ (proton), $-{}^1/_2 \leftrightarrow {}^1/_2$ electron spin transition. Common parameters are $a_{iso} = 0$ MHz, $T_\perp = -3$ MHz, $B_o = 6100$ G. In trace 1 $D/g\beta = 0$. In traces 2, 3, and 4 the angle θ_{hc} is 0°, 45°, and 90°, respectively, and $D/g\beta$ is Gaussian-distributed around the central value of 400 G, with the distribution width (between the maximal slope points) of 200 G. Labels "$A_{||}$" and "$A_\perp$" mark the features corresponding to, respectively, parallel and perpendicular orientations of the hfi axis relative to $\mathbf{B_o}$.

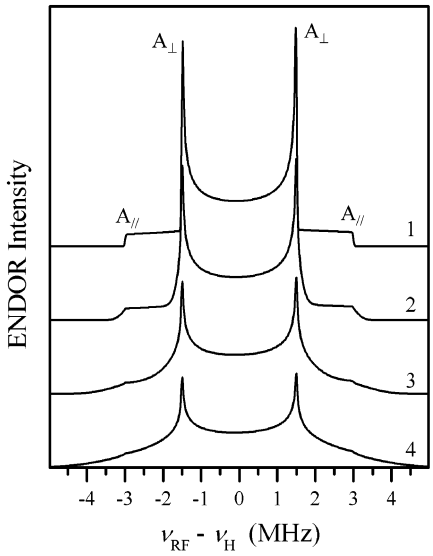

Figure 4. Calculated CW ENDOR spectra for an orientationally disordered system with $S = {}^7/_2$, $I = {}^1/_2$ (proton), $-{}^1/_2 \leftrightarrow {}^1/_2$ electron spin transition. Common parameters are $a_{iso} = 0$ MHz, $T_\perp = -3$ MHz, $B_o = 6100$ G. In trace 1 $D/g\beta = 0$. In traces 2, 3, and 4 $D/g\beta$ is Gaussian-distributed around the central values of 200 G, 400, and 600 G, respectively. The respective $D/g\beta$ distribution widths (between the maximal slope points) are 100, 200, and 300 G. The angle θ_{hc} is distributed within the limits from 0° to 90°. The statistical weight of an orientation with a given θ_{hc} is taken as sin θ_{hc}, which corresponds to the model of a complex with many ligand protons at various orientations. Labels "$A_{||}$" and "$A_\perp$" mark the features corresponding to, respectively, parallel and perpendicular orientations of the hfi axis relative to $\mathbf{B_o}$.

Fortunately, however, the cfi parameters in glassy samples are always statistically distributed in broad limits,[32−34] which leads to a great simplification of the spectroscopic situation. As an example, Figure 3 shows the spectra calculated for distributed D-values and fixed angles θ_{hc}. Comparison with Figure 2 shows that the cfi distribution eliminates most of the additional singularities, and the spectral shapes become considerably closer to the usual powder pattern calculated without the cfi (trace 1 in Figure 3). The $A_\perp$ peaks in these spectra become the dominant features, but the spectra remain significantly distorted and asymmetric, and their shoulders show noticeable shifts from the true $A_{||}$ positions.

In addition to the distribution of the cfi parameters, the relative orientations of hfi and cfi tensors can also be distributed. If the cfi tensor orientation is fixed in the molecular frame but the Gd complex has many ligand protons with similar hfi parameters (like the Gd^{3+} aquo complex), then the hfi tensors of these protons will have various orientations relative to the cfi tensor. From the ENDOR standpoint, the situation is then practically identical (apart from the intensity of the ENDOR lines) to that of having a single proton and a statistically distributed angle θ_{hc}.

Figure 4 shows the spectra calculated for various distributions of D-values and for the angle θ_{hc} being distributed within the limits from 0° to 90°. The distribution over θ_{hc} results in symmetric spectra resembling the spectrum calculated for $D = 0$ (trace 1 in Figure 4). Importantly, the distributions in D and θ_{hc} eliminate all the spectral singularities other than those pertaining to $A_{||}$ and $A_\perp$. In all the spectra $A_\perp$ peaks remain the prominent features. The $A_{||}$ shoulders, however, become progressively broader with increasing D and its distribution width. In such a situation, neglecting the effect of cfi will result in an overestimation of $A_{||}$ and, as a result, in some overestimation of both $T_\perp$ and a_{iso}. For example, the splitting between the half-height points of the shoulders in trace 3 (central $D/g\beta = 400$ G) is about 6.9 MHz. If this splitting is taken as $A_{||}$, then $T_\perp = -3.3$ MHz and $a_{iso} = 0.3$ MHz can be estimated, although the true values used in the simulation are $T_\perp = -3$ MHz and $a_{iso} = 0$ MHz.

Another effect of cfi is not related to the distortions of ENDOR spectra within each electron spin manifold but rather to the fact that in an ENDOR experiment several different EPR transitions may be involved. For example, the center of the EPR spectrum of Gd^{3+} has contributions from all possible transitions: $-{}^1/_2 \leftrightarrow {}^1/_2$, $\pm{}^1/_2 \leftrightarrow \pm{}^3/_2$, $\pm{}^3/_2 \leftrightarrow \pm{}^5/_2$, and $\pm{}^5/_2 \leftrightarrow \pm{}^7/_2$. In such a situation the conventional 1D ENDOR spectrum will be a superposition of spectra of nuclear transitions within each of the contributing electron spin manifolds. If there is a distribution of the angles θ_{hc}, the spectra that belong to the manifolds with $m_Z = \pm{}^N/_2$ will be approximately (neglecting the distortions due to the cfi) similar to the spectra for the manifolds with $m_Z = \pm{}^1/_2$ but extended along the frequency axis so that all the ENDOR splittings are N times greater than those for the $m_Z = \pm{}^1/_2$ manifolds. Such contributions were described in detail for the Mn^{2+} aquo complex with a weak cfi.[35] Therefore, we will not discuss them here but will only mention that their presence may (and does, as we will see below) lead to serious difficulties in extracting hfi parameters from 1D ENDOR spectra.

The problem may be simplified by using a combination of a high mw frequency (W-band or higher) and low temperature (<2 K) in order to selectively populate the lowest energy electron spin manifold (the one with $m_Z = -S$), which will result in ENDOR spectra contributed by two manifolds only (those with $m_Z = -S$ and $m_Z = -S + 1$).[32] Even with selective population, however, the overlapping spectra may be difficult to interpret in some cases, and their separation may be required.

3.3. 2D Mims ENDOR. One of the techniques capable of disentangling the ENDOR spectra that belong to different electron spin manifolds is Mims ENDOR,[26,27] although, to our

knowledge, it has never been used for such a purpose. Mims ENDOR is based on a stimulated electron spin−echo (ESE) sequence that consists of three 90° mw pulses, with the first two pulses being separated by time interval τ and the second two pulses being separated by time interval T. The RF pulse is applied during the interval T, and the stimulated ESE amplitude is recorded as a function of the RF carrier frequency, ν_{RF}, and time interval τ. The Mims ENDOR response (which is the difference between the stimulated ESE amplitudes with and without the RF pulse) is an oscillating function of τ[26]

$$\Delta V(\nu_{RF}, \tau) \propto [1 - \cos 2\pi(\nu_1 - \nu_2)\tau][\delta(\nu_{RF} - \nu_1) + \delta(\nu_{RF} - \nu_2)] \quad (9)$$

where ν_1 and ν_2 are the nuclear transition frequencies within the electron spin manifolds involved in an EPR transition used for detecting ENDOR. The Fourier transformation (FT) of the τ-dependence results in a 2D Mims ENDOR spectrum

$$\Delta V(\nu_{RF}, \nu_\tau) \propto \delta(\nu_\tau - \Delta\nu_{12})[\delta(\nu_{RF} - \nu_1) + \delta(\nu_{RF} - \nu_2)] \quad (10)$$

where ν_τ is the frequency corresponding to the time interval τ and $\Delta\nu_{12} = |\nu_1 - \nu_2|$. In this 2D spectrum the nuclear transitions will appear as peaks located at the frequencies (ν_1, $\Delta\nu_{12}$) and (ν_2, $\Delta\nu_{12}$).

For the case of weak hfi and axial cfi we can use eq 7 to find an approximate expression for $\Delta\nu_{12}$

$$\Delta\nu_{12} \approx \left| a_{iso} + T_{ZZ} + \frac{3Dc_{\theta_C}s_{\theta_C}}{g\beta B_o}(2m_Z + 1)(c_{\varphi_C}T_{XZ} + s_{\varphi_C}T_{YZ}) \right| \quad (11)$$

where we assumed that the EPR transition occurs between the manifolds with m_Z and $m_Z + 1$. For $S = {}^1/_2$ (no cfi) $\Delta\nu_{12} \approx a_{iso} + T_{ZZ}$ and does not depend on ν_I, whereas ν_1 and ν_2 have a ν_I dependence (see eq 7). This property of 2D Mims ENDOR spectra can be used to disentangle the contributions of nuclei with different Zeeman interactions, even if they give overlapping 1D ENDOR spectra (e.g., ^{1}H and ^{19}F or ^{1}H and strongly coupled ^{14}N), as was demonstrated elsewhere by employing a hyperfine-correlated ENDOR (HYEND)[36] that produces 2D spectra similar to those of 2D Mims ENDOR.

For $S > {}^1/_2$, neglecting the cfi contributions to $\Delta\nu_{12}$ and $\nu_{1,2}$, we may deduce that the lines in the ^{1}H 2D Mims ENDOR spectrum will be located at the frequencies $\nu_{RF} \approx \nu_H - (a_{iso} + T_{ZZ})m_Z$ and $\nu_\tau \approx a_{iso} + T_{ZZ}$. One can see that in this approximation the value of ν_τ does not depend on m_Z. Therefore, the correlation lines in the 2D spectrum that pertain to a given hfi constant $A = a_{iso} + T_{ZZ}$ but different m_Z values will all be located at the same frequency $\nu_\tau \approx A$, although the frequencies ν_{RF} for them will be different. Conversely, if two protons have different hfi values, A_1 and A_2, and the ENDOR frequencies ν_{RF} for these nuclei coincide for some of the m_Z values (i.e., $\nu_H - A_1m_{Z1} = \nu_H - A_2m_{Z2}$), then these two transitions can still be disentangled in the 2D Mims ENDOR spectrum because they will have different frequencies ν_τ.

Including the cfi term will result in deviations of both ν_{RF} (for any m_Z) and ν_τ (for $m_Z \neq -{}^1/_2$, that is, for all EPR transitions except the one between $m_Z = {}^1/_2$ and $-{}^1/_2$; see eq 11) from the approximate values discussed above. The scale of these deviations, as well as overall 2D spectral line shapes, can be assessed using numerical simulations. The results of such simulations are presented in Figure 5 that shows 2D plots ($\nu_{RF} - \nu_H$ vs. ν_τ) calculated for the same hfi parameters as those used in Figure 2. Panels a−d in this figure correspond to the EPR transition $-{}^1/_2 \leftrightarrow {}^1/_2$, whereas panels e−h correspond to the ${}^1/_2 \leftrightarrow {}^3/_2$ EPR transition. In panels a and e the D-value is equal to zero, whereas in panels b and f $D/g\beta = 400$ G and $\theta_{hc} = 90°$. In panels c, d, g, and f the D-value and θ_{hc} are distributed.

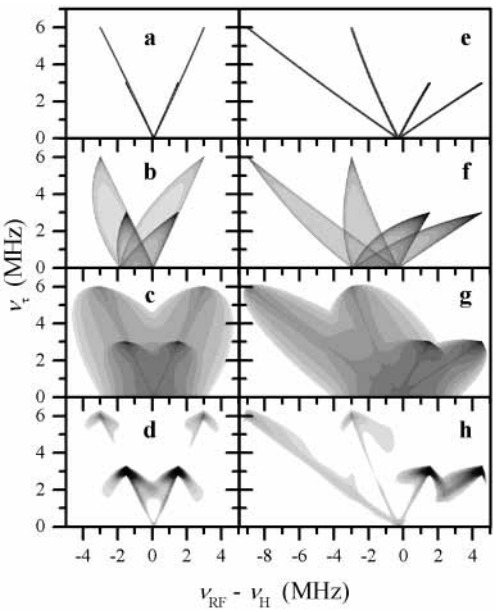

Figure 5. Calculated 2D Mims ENDOR spectra in an orientationally disordered system with $S = {}^7/_2$, $I = {}^1/_2$ (proton), $-{}^1/_2 \leftrightarrow {}^1/_2$ (left column) and ${}^1/_2 \leftrightarrow {}^3/_2$ (right column) electron spin transitions. Common parameters are $a_{iso} = 0$ MHz, $T_\perp = -3$ MHz, $B_o = 6100$ G. In panels a and e $D/g\beta = 0$. In panels b and f $D/g\beta = 400$ G and $\theta_{hc} = 90°$. In panels c, g, d, and h $D/g\beta$ is Gaussian-distributed around the central value of 400 G, with the width between the maximal slope points of 200 G and θ_{hc} is distributed within the limits from 0° to 90°. The statistical weight of an orientation with a given θ_{hc} is taken as sin θ_{hc}, which corresponds to the model of a complex with many ligand protons at various orientations. Spectra c and g correspond to zero dead time. Spectra d and h correspond to a dead time of 200 ns.

Figure 5 demonstrates that, despite all the broadening and distortions of 2D Mims ENDOR spectra by the cfi, there are convergence points at the spectral positions corresponding to canonical orientations of the hfi tensor. In the case of a distributed cfi and θ_{hc} they represent the only remaining singularities observed in 2D spectra. The cfi contribution to the frequencies at these points equals zero (see eqs 7 and 11), and the peak positions are determined by the Zeeman and hf interactions. If an experiment is performed without refocusing of the ESE signal[37] there will be an appreciable dead time in τ-dependences, usually on the order of 100−200 ns. The broad spectral components corresponding to a fast-damping oscillation may decay within the dead time. As a result, after the FT of the τ-dependences, the convergence points that correspond to a slow-damping oscillation will be accentuated. This is illustrated by panels d and h of Figure 5 that correspond to panels c and g of Figure 5, respectively, but are obtained by FT of τ-dependences with a dead time of 200 ns.

The 2D spectra in panels c, d, g, and h of Figure 5 were simulated with an averaging over both the D-value and θ_{hc}. It is not necessary, however, to have both of the distributions in order to obtain the 2D spectra with the intensity enhancements at the canonical orientations of the hfi tensor. The simulations with separate averagings over θ_{hc} or over D are shown in Figure 6. Similar results were obtained for a general rhombic cfi tensor (not shown). Thus, panels d and h of Figure 5, as well as panels e−h of Figure 6, represent the kind of spectra one can expect

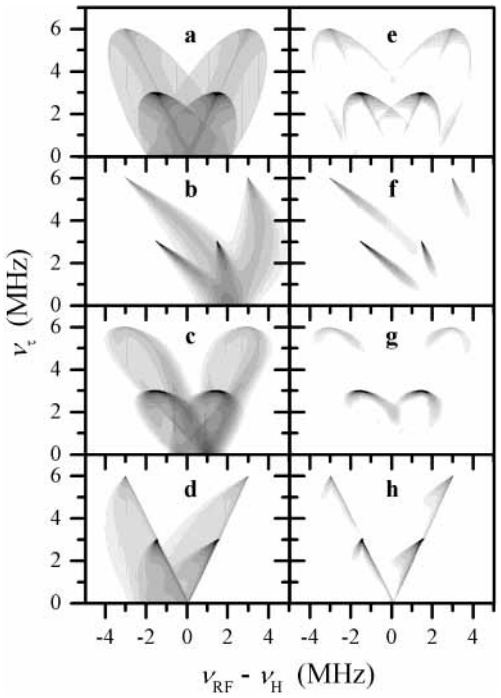

Figure 6. Calculated 2D Mims ENDOR spectra in an orientationally disordered system with $S = {}^7/_2$, $I = {}^1/_2$ (proton), $-{}^1/_2 \leftrightarrow {}^1/_2$ electron spin transition. Common parameters are $a_{iso} = 0$ MHz, $T_\perp = -3$ MHz, $B_o = 6100$ G. In panels a and e $D/g\beta = 400$ G and θ_{hc} is distributed within the limits from 0° to 90° (the statistical weight of an orientation with a given θ_{hc} is taken as sin θ_{hc}, which corresponds to the model of a complex with many ligand protons at various orientations). In all other panels $D/g\beta$ is Gaussian-distributed around the central value of 400 G, with the width between the maximal slope points of 200 G. In panels b and f $\theta_{hc} = 0°$. In panels c and g $\theta_{hc} = 45°$. In panels d and h $\theta_{hc} = 90°$. Spectra a−d correspond to zero dead time. Spectra e−h correspond to a dead time of 200 ns.

to obtain in a real 2D Mims ENDOR experiment for a system that does not show an excessively broad static distribution of the hfi parameters. The singularities in these spectra can be used to estimate the hfi parameters in glassy samples of Gd^{3+} complexes even without knowing the details of the distribution of the cfi parameters.

The Gd^{3+} aquo complex corresponds to the situation with distributed cfi parameters and relative orientations of the cfi and hfi tensors. For the MRI contrast agent Gd^{3+}HPDO3A the effective angle θ_{hc} is also likely to be distributed in broad limits (in addition to the cfi distribution) because of the electronic asymmetry and structural flexibility of the HPDO3A ligand,[1] the possibility of asymmetric realizations of its hydrogen bonding, the rotational (around the Gd−O bond) degree of freedom of the H_2O ligand, and the presence of an additional hydroxyl proton that belongs to the hydroxypropyl arm of the HPDO3A ligand. This proton is located at about the same distance from the Gd ion as the water ligand protons, but its position in the complex depends on the conformation of the hydroxypropyl arm.

4. Experimental Results and Discussion

4.1. ESE Field Sweeps and 1D Mims ENDOR Spectra. Figure 7 shows the primary electron spin−echo (ESE) field sweeps for the Gd^{3+} aquo complex (trace 1) and Gd^{3+}HPDO3A (trace 2). The shape of these spectra is typical for Gd^{3+} complexes characterized by weak cfi.[33] Mims ENDOR experiments were performed at magnetic fields corresponding to the maximal contribution of $-{}^1/_2 \leftrightarrow {}^1/_2$ EPR transition (labeled A in Figure 7) and maximal contribution of $\pm{}^1/_2 \leftrightarrow \pm{}^3/_2$ EPR transitions (labeled B in Figure 7). The 1D ENDOR spectra obtained at these positions are shown in Figure 8. We will consider first the spectra of the Gd^{3+} aquo ion (top traces) because they are more simple.

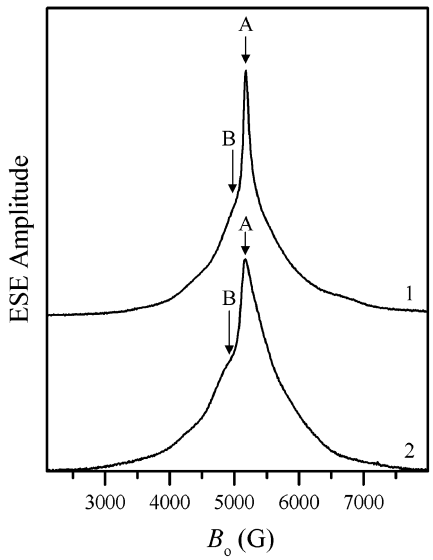

Figure 7. Two-pulse ESE field sweep spectra of Gd^{3+} aquo complex (trace 1) and Gd^{3+}HPDO3A (trace 2) in frozen glassy water/methanol solutions. Experimental conditions: mw frequency ν_{mw}, 14.411 GHz; mw pulse durations, 10 ns; time interval τ between the mw pulses, 130 ns; temperature, 4.2 K. Labels "A" and "B" mark the spectral positions where ENDOR spectra were recorded. Position A corresponds to a maximal contribution of the $-{}^1/_2 \leftrightarrow {}^1/_2$ EPR transition. At position B the transitions $\pm{}^1/_2 \leftrightarrow \pm{}^3/_2$ contribute the most. The B_o values corresponding to positions A are 5177 G in both spectra. Position B in spectrum 1 corresponds to $B_o = 4980$ G, whereas in spectrum 2 it corresponds to $B_o = 4920$ G.

The 1D ENDOR spectrum of the Gd^{3+} aquo ion obtained at the B_o value corresponding to position A (solid trace in the top group of traces in Figure 8), apart from minor details, looks very similar to a usual ENDOR spectrum of a paramagnetic center with $S = {}^1/_2$. The central broad peak in this spectrum arises from distant matrix protons. Two sharp lines marked "$A_{1\perp}$" belong to protons of the water molecules coordinated to Gd ions. The splitting between these lines is $A_{1\perp} = -2.62 \pm 0.02$ MHz, and it corresponds to the 90° angle between $\mathbf{B_o}$ and the direction of the main hfi axis (here and below the sign of $A_{1\perp}$ is chosen to be negative because, based on single-crystal ENDOR results[23,24] and on our discussion above, $A_{1\perp}$ is dominated by the negative anisotropic hfi constant, $T_\perp$, that is determined by a through-space dipolar interaction between the protons and the unpaired electrons of Gd^{3+}). The shoulders marked "$A_{1||}$" with a splitting between them of $A_{1||} = 5.5 \pm 0.1$ MHz also belong to ligand water protons but correspond to the orientation of the hfi tensor axis being about parallel to $\mathbf{B_o}$. The $A_{1\perp}$ and $A_{1||}$ features correspond to the proton transitions within the electron spin manifolds with $m_Z = \pm{}^1/_2$.

The only features that make this spectrum different from those of a usual $S = {}^1/_2$ system are the peaks marked "$3A_{1\perp}$". The splitting between these peaks is about 7.8 MHz, or about 3 times greater than $A_{1\perp}$. The peaks $3A_{1\perp}$ obviously belong to the transitions of ligand water protons within the electron spin manifolds with $m_Z = \pm{}^3/_2$. To prove this assertion, the ENDOR spectrum was also measured at the B_o value corresponding to position B of the EPR spectrum 1 in Figure 7. In this spectrum (dashed trace in the upper group of traces in Figure 8), as expected, the amplitude of the $A_{1\perp}$ and $A_{1||}$ features decreased

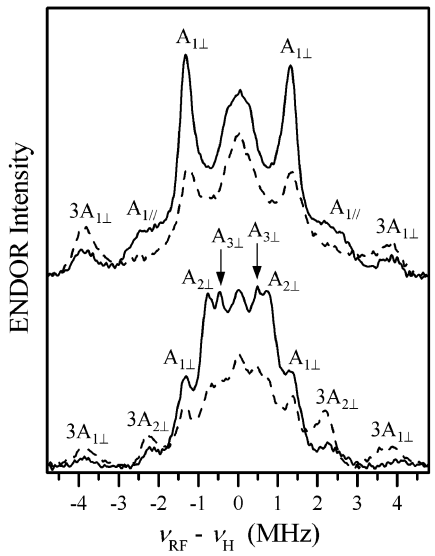

Figure 8. 1D Mims ENDOR spectra of the Gd^{3+} aquo complex (top traces) and Gd^{3+}HPDO3A (bottom traces) in frozen glassy water/methanol solutions. Solid and dashed traces are recorded at, respectively, positions A and B of the EPR spectra shown in Figure 7 and normalized by the ESE signal amplitudes observed without an RF pulse. Experimental conditions: mw frequency ν_{mw}, 14.411 GHz; mw pulse durations, 10 ns; time interval τ between the first and second mw pulses, 130 ns; time interval T between the second and third mw pulses, 30 μs; RF pulse duration, 21 μs; temperature, 4.2 K. Labels "$A_{1//}$" and "$A_{1\perp}$" mark the features of the lines of ligand proton transitions within $m_Z = \pm 1/2$ electron spin manifolds corresponding to, respectively, parallel and perpendicular orientations of the proton hfi axes relative to $\mathbf{B_0}$. Labels "$3A_{1\perp}$" mark the features of the lines of ligand proton transitions within $m_Z = \pm 3/2$ electron spin manifolds corresponding to the perpendicular orientation of the proton hfi axes relative to $\mathbf{B_0}$. Labels "$A_{2\perp}$", "$3A_{2\perp}$" and "$A_{3\perp}$" have the same meanings, but refer to the lines of second-sphere protons.

and that of the $3A_{1\perp}$ features increased. The small relative intensity of the $3A_{1\perp}$ peaks is explained by the fact that the width of the ENDOR lines is proportional (and therefore the intensity is inversely proportional) to m_Z and, in addition, that the EPR lines corresponding to the $\pm 1/2 \leftrightarrow \pm 3/2$ and $\pm 3/2 \leftrightarrow \pm 5/2$ transitions are broader, respectively, than the lines of the $-1/2 \leftrightarrow 1/2$ and $\pm 1/2 \leftrightarrow \pm 3/2$ transitions, as was discussed in the Theoretical Background.

Neglecting the effect of the cfi on the shape of the ENDOR spectrum, we can use the splittings $A_{1\perp} = a_{iso} + T_\perp \approx -2.62 \pm 0.02$ MHz and $A_{1||} = a_{iso} - 2T_\perp \approx 5.5 \pm 0.1$ MHz to estimate the isotropic hfi constant $a_{iso} \approx 0.08 \pm 0.02$ MHz and the anisotropic hfi constant $T_\perp \approx -2.70 \pm 0.04$ MHz. The presence of cfi, as discussed in the theoretical section, mostly results in an increase of the observable splitting between the $A_{1||}$ features. Taking this effect into account may result in slightly smaller a_{iso} and $|T_\perp|$ values.

The solid and dashed traces shown at the bottom of Figure 8 are the Mims ENDOR spectra of Gd^{3+}HPDO3A. Unlike the Gd^{3+} aquo complex, this complex has only one accessible site for water coordination. In addition, as mentioned above, the HPDO3A ligand contains an OH group directly coordinated to Gd (see Figure 1), and the proton of this group is likely to have hfi parameters similar to those of the water ligand. The lines corresponding to these immediate ligand protons are marked "$A_{1\perp}$", as those for the Gd^{3+} aquo complex, and the splitting between these lines is also about -2.65 MHz. It would be tempting to assign the features with a splitting of about 4.5−5 MHz to $A_{1||}$ (and mark them "$A_{1||}$"), but a close examination of the spectra of Gd^{3+}HPDO3A prevents us from doing so.

The problem is related to the fact that the HPDO3A ligand contains numerous CH_2 groups. In addition, there are multiple oxygen and nitrogen atoms capable of hydrogen bonding with protons of solvent water molecules**.** These second-sphere hydrogens are located further away from the central ion than those covalently attached to immediate ligand atoms but not sufficiently far away as to be indistinguishable from distant matrix hydrogens. Indeed, the spectrum of Gd^{3+}HPDO3A shows additional lines marked "$A_{2\perp}$" and "$A_{3\perp}$" that correspond to the perpendicular orientation of the hfi tensors of the second-sphere protons with respect to $\mathbf{B_0}$. The hfi constants $A_{2\perp}$ and $A_{3\perp}$ are approximately equal to -1.5 and -0.93 MHz, respectively. As was previously mentioned, and shown for the Gd aquo complex, the isotropic hfi constant for the direct ligand protons is close to zero, and this should be true for the second-sphere protons. Therefore, the observed splittings $A_{2\perp}$ and $A_{3\perp}$ are taken as a direct measure of the anisotropic hfi constants $T_{2\perp}$ and $T_{3\perp}$, and distances of about 3.75 Å and 4.4 Å, respectively, can be estimated. The distance of 3.75 Å is close to that expected for the solvent protons hydrogen-bonded to the oxygen and nitrogen atoms coordinated to the Gd^{3+} ion. On the other hand, the distance of 4.4 Å approximately corresponds to that between Gd^{3+} and the methylene protons of the complex.

It is easy to see that the hf splitting $|3A_{2\perp}|$ (corresponding to proton transitions within the electron spin manifolds with $m_Z = \pm 3/2$) is equal to about 4.5 MHz, as the splitting between the weak features in the ENDOR spectrum that we intended to assign to $A_{1||}$. In the ENDOR spectrum recorded at the EPR position B (dashed bottom trace in Figure 8) the amplitude of these features has increased compared to that in the spectrum recorded at the EPR position A. This shows that, indeed, these features are dominated by proton transitions within the electron spin manifolds with $m_Z = \pm 3/2$, and therefore they are marked "$3A_{2\perp}$" in Figure 8.

From the above considerations we conclude that we cannot observe $A_{1||}$ features in the ENDOR spectrum of Gd^{3+}HPDO3A. As a result, we cannot independently estimate a_{iso} and $T_\perp$ from this spectrum. Although it is reasonable to assume that a_{iso} is close to zero, our single example with the Gd aquo ion does not give us any information regarding the possible range of a_{iso} variation. Because we would like to determine the hfi parameters with the highest possible accuracy rather than assume what their values could be, we need to disentangle the contributions to the ENDOR spectrum of nuclear transitions belonging to different m_Z and to observe the $A_{1||}$ features directly. As shown in the theoretical section, this can be accomplished using the 2D Mims ENDOR.

4.2. 2D Mims ENDOR Spectra. Figure 9 shows the 2D Mims ENDOR spectrum of Gd^{3+} aquo ion. The peaks observed in this spectrum are labeled the same way as the corresponding features in the 1D spectrum in Figure 8. The inner parts of the topmost contour lines are shaded to show the location of maximum of each feature. One can see that the features $A_{1\perp}$ and $A_{1||}$ corresponding to nuclear spin transitions within the $m_Z = \pm 1/2$ electron spin manifolds are located along the dashed lines labeled "1/2". For these features the oscillation frequencies ν_τ are equal to $A_{1\perp}$ and $A_{1||}$, respectively. The features $3A_{1\perp}$ corresponding to $m_Z = \pm 3/2$ are located along the dashed lines labeled "3/2". The frequencies ν_τ for $3A_{1\perp}$ peaks are equal to $A_{1\perp}$, as those for $A_{1\perp}$ peaks.

Finally, two weak features located between the $A_{1||}$ lines also belong to the nuclear transitions with $A_{1\perp}$. The ν_τ frequency for them, however, equals to $2A_{1\perp}$. This indicates that these lines correspond to a simultaneous RF-induced flip of an even number

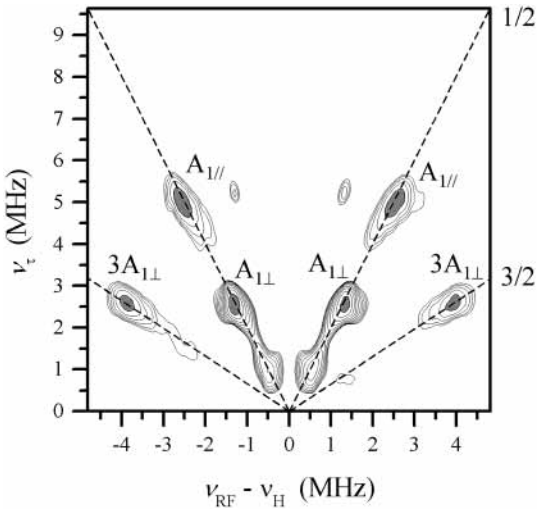

Figure 9. 2D Mims ENDOR spectrum of Gd^{3+} aquo ion in frozen glassy water/methanol solution. Experimental conditions: mw frequency $\nu_{mw} = 17.140$ GHz; magnetic field $B_o = 6147$ G (this combination of ν_{mw} and B_o is the same as that defined by point A in the field sweep spectrum of Figure 7); mw pulse durations, 10 ns; starting time interval τ between the first and second mw pulses, 130 ns (this is the dead time of this experiment); time interval T between the second and third mw pulses, 30 μs; RF pulse duration, 18 μs; temperature, 4.2 K. Labels "$A_{1||}$", "$A_{1\perp}$" and "$3A_{1\perp}$" have the same meaning as in Figure 8. Dashed diagonal lines marked "1/2" and "3/2" are the lines along which the spectral features belonging to the electron spin manifolds with $|m_Z| = {}^1/_2$ and $|m_Z| = {}^3/_2$ are situated.

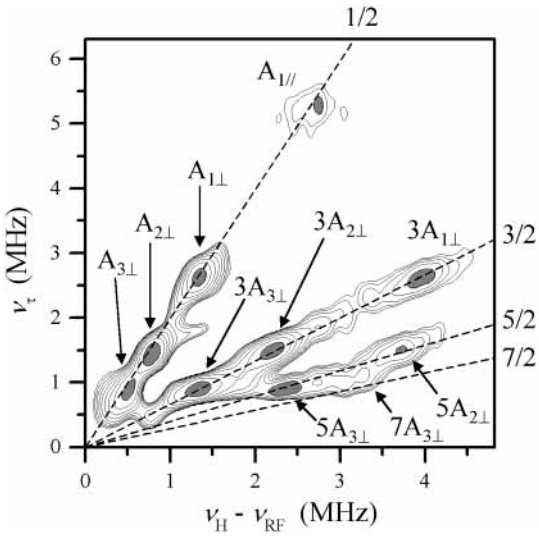

Figure 10. 2D Mims ENDOR spectrum of Gd^{3+}HPDO3A MRI contrast agent in frozen glassy water/methanol solution. Experimental conditions are the same as in Figure 9. Labels showing the transition assignments (e.g., "$A_{1||}$", "$A_{1\perp}$", "$3A_{1\perp}$") have the same meaning as in Figure 8. Note also that proton transitions within the electron spin manifolds with $|m_Z| = {}^5/_2$ (marked, e.g., "$5A_{3\perp}$") are clearly seen, and there is an indication of the transition that belongs to $|m_Z| = {}^7/_2$ (marked "$7A_{3\perp}$"). Dashed diagonal lines marked "1/2" through "7/2" are the lines along which the spectral features belonging to the electron spin manifolds with $|m_Z|$ from $^1/_2$ to $^7/_2$ are situated.

of nuclear spins.[27,38] It is rather unusual to observe such multinuclear effects in ENDOR spectra because they require the paramagnetic center to have a large number of protons with similar hfi parameters. This condition is obviously satisfied for the Gd^{3+} aquo ion.

The $A_{1\perp}$ and $A_{1||}$ splittings in the 2D spectrum are -2.64 ± 0.02 MHz and 5.15 ± 0.1 MHz, respectively, which results in hfi parameters $a_{iso} \approx -0.04 \pm 0.02$ MHz and $T_\perp \approx -2.60 \pm 0.04$ MHz. One can see that although the $A_{1\perp}$ splitting in the 2D spectrum is practically the same as that in the 1D spectrum of Figure 8, the $A_{1||}$ splitting has decreased by 0.35 MHz (5.15 MHz vs 5.5 MHz), which leads to a slightly different hfi estimate.

Figure 10 shows the 2D Mims ENDOR spectrum of the contrast agent Gd^{3+}HPDO3A. In this case the number of close ligand protons was considerably smaller and, correspondingly, the intensity of their ENDOR lines was weaker. Therefore, to reach a sufficient signal-to-noise ratio in reasonable time, we accumulated only one-half of the spectrum (the one for $\nu_{RF} \leq \nu_H$). The assignments of various line maxima are shown in the figure. One can see that in this case not only the nuclear transitions within $|m_Z| = {}^3/_2$ electron spin manifolds are observed, but also the transition of second-sphere protons within $|m_Z| = {}^5/_2$ and $|m_Z| = {}^7/_2$ manifolds falls into the shown spectral range. The lines $A_{1\perp}$ and $A_{1||}$ are now well separated from all other lines, and their maxima correspond to $A_{1\perp} \approx -2.66 \pm 0.03$ MHz and $A_{1||} \approx 5.30 \pm 0.25$ MHz (the error limits here are considerably wider than in the case of Gd^{3+} aquo ion because of smaller signal intensity). The hfi parameters found from these line positions are $a_{iso} = -0.01 \pm 0.06$ MHz, $T_\perp = -2.65 \pm 0.09$ MHz.

4.3. Refined hfi Parameters and Their Static Distributions. So far we have only used the positions of the $A_{1\perp}$ and $A_{1||}$ features in 1D and 2D ENDOR spectra to estimate the values of isotropic and anisotropic hfi constants. Additional information about these parameters can be obtained from an analysis of the width of the ENDOR spectral lines. Numerical simulations show that in order to reproduce the experimental width of $A_{1\perp}$ peaks in the 1D spectra of Gd^{3+} aquo ion, either a_{iso} or $T_\perp$ has to be Gaussian-distributed with the width between the maximal slope points of about 0.4 MHz. In principle, the distribution of $T_\perp$ should lead to a twice greater broadening of $A_{1||}$ than the distribution of a_{iso}. However, because the shape of $A_{1||}$ shoulders in 1D spectra is also determined by the distributed cfi (average $D/g\beta \sim 300$ G, as estimated from the field sweep spectrum in Figure 7), both hfi distributions result in very similar simulated 1D spectra. Simulation of 2D Mims ENDOR spectra also did not allow us to distinguish between these two distributions, primarily because of rather low resolution determined by the short transverse relaxation time T_2 of about 900 ns.

On the other hand, correlated distributions of a_{iso} and $T_\perp$, where the changes of these parameters added up at $A_{1||}$ and partly (as to provide the residual broadening of 0.4 MHz) offset each other at $A_{1\perp}$, clearly produced too broad $A_{1||}$ shoulders if the distribution width for $T_\perp$ exceeded 0.5 MHz. This value can be used, therefore, as a maximal possible distribution width of $T_\perp$ that would not contradict our experimental results.

Apart from estimating the distribution width for hfi parameters, the simulations have allowed us to obtain corrected values of the central (or average) hfi parameters: $a_{iso} = 0.03 \pm 0.02$ MHz and $T_\perp = -2.67 \pm 0.04$ MHz. As an example, Figure 11 shows 1D spectra of Gd^{3+} aquo ion simulated with distributed hfi parameters (trace 1 reproduces the experimental spectrum of Gd^{3+} aquo ion shown in Figure 8, trace 2 is simulated with distributed a_{iso}, trace 3 is simulated with distributed $T_\perp$, and trace 4 is simulated with a correlated distribution of a_{iso} and $T_\perp$ as explained above and in the figure caption). One can see that traces 2 and 3 that correspond to distribution widths of $T_\perp$ of 0 and 0.4 MHz, respectively, are practically indistinguishable. On the other hand, in trace 4 that corresponds to the $T_\perp$ distribution width of 0.8 MHz the $A_{1||}$ shoulders become significantly more broad than those observed in experiment. The Gd−H distance

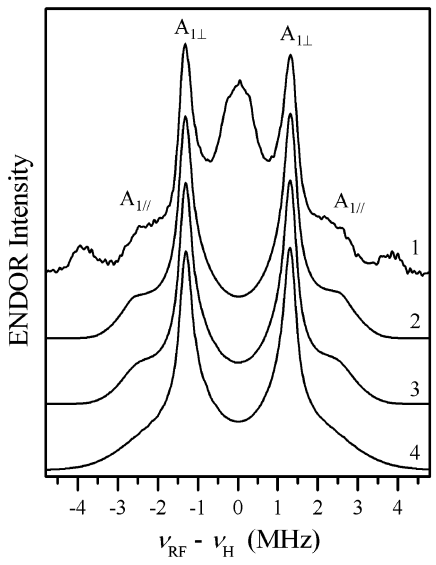

Figure 11. 1D Mims ENDOR spectra of Gd^{3+} aquo complex. Trace 1 is experimental (reproduced from Figure 8, top solid trace). Traces 2−4 are simulated (for the $-1/2 \leftrightarrow 1/2$ electron spin transition) with distributed hfi and cfi parameters. In all simulated traces the central hfi and cfi values were $a_{iso} = 0.03$ MHz, $T_\perp = -2.67$ MHz, $D/g\beta = 300$ G and the cfi parameter $D/g\beta$ was Gaussian-distributed around the central value with the width between the maximum slope points of 150 G. Angle θ_{hc} between the hfi and cfi axes was distributed within the limits from 0° to 90°. In trace 2 a_{iso} was distributed while $T_\perp$ was kept fixed. In trace 3 a_{iso} was kept fixed while $T_\perp$ was distributed. The Gaussian distribution width for the distributed hfi parameter in traces 2 and 3 was 0.4 MHz. In trace 4 both a_{iso} and $T_\perp$ were distributed with the distribution widths of 0.4 and 0.8 MHz, respectively. The distributions were correlated so that an increase or decrease of a_{iso} corresponded, respectively, to a decrease or increase of $T_\perp$ (as $T_\perp < 0$, an increase in $T_\perp$ corresponds to a decrease in $|T_\perp|$). Labels "$A_{1||}$" and "$A_{1\perp}$" have the same meaning as in Figure 8.

that corresponds to the central value of $T_\perp \approx -2.67 \pm 0.04$ MHz is $R_{GdH} \approx 3.09 \pm 0.02$ Å.

As follows from 1D ENDOR spectra, the hfi distribution width for GdHPDO3A is similar to that for Gd aquo ion, ~0.4 MHz. The simulations of a 2D Mims ENDOR spectrum with such an hfi distribution width result in the central hfi parameters $a_{iso} = 0.04 \pm 0.06$ MHz and $T_\perp = -2.75 \pm 0.09$ MHz. The Gd−H distance that corresponds to $T_\perp \approx -2.75 \pm 0.09$ MHz is $R_{GdH} \approx 3.06 \pm 0.04$ Å.

4.4. Origin of Static hfi Distribution. We have estimated above the characteristic width of static hfi distribution of about 0.4 MHz but were unable to tell, based solely on our experimental data, which distribution of the hfi parameters (a_{iso} or $T_\perp$) mainly contributes to this width. We can, however, obtain some clues on this issue from appropriate published data.

First, analysis of the hfi data for ^{19}F nuclei in complexes of fluorine with rare earth ions (Tm^{2+}, Yb^{3+}, Eu^{2+})[29,39] shows that the spin density delocalized on a fluorine ligand is about 0.2 ± 0.1%. This gives us an approximate value of a spin density that we may reasonably expect to be delocalized on an oxygen ligand in the Gd^{3+} complexes. In a pertinent investigation of Cu^{2+} complexes, isotropic hfi constants for protons of water molecules coordinated to Cu^{2+} were found to be $|a_{iso}| \leq 1.4$ MHz,[40] whereas the average spin density transferred to oxygen was found to be about 5.5%.[41] Since for both ions, Gd^{3+} and Cu^{2+}, the spin density is delocalized to the ligand through a σ-bond, we can expect proton hfi constants a_{iso} to scale with the spin densities on oxygen with similar proportionality factors. Combining the above data we can therefore estimate possible isotropic hfi constants for protons in Gd−water complexes as $|a_{iso}| \sim 0.05 \pm 0.03$ MHz, which is very close to the average hfi constants obtained in our experiments. The hfi constant $|a_{iso}| \sim 0.025$ MHz can also be estimated for water ligand protons from the ^{17}O hfi constant of ~ -0.6 MHz obtained by ^{17}O NMR of Gd^{3+} complexes with different coligands.[6−8] In addition, Bryden et al.[42] separated the contact and pseudocontact contributions to the chemical shift of deuterons of the D_2O ligand in $[Ln(DOTA)(D_2O)]^-$ and the lanthanide aquo ions and estimated $a_{iso} \approx 0.075$ MHz for the protons of water ligands bound to GdDOTA (an analogue of HPDO3A) and $a_{iso} \approx 0.005$ MHz for the waters bound to the aquo ion.

If we assign the whole characteristic width of hfi variation found in this work (0.4 MHz) to a_{iso} only, then values of a_{iso} at least as large as 0.25 MHz will be possible, which would translate to the oxygen spin densities of about 1%. In view of the experimental data for fluorine complexes and NMR data such large spin densities on oxygen seem to be unrealistic. We must conclude therefore that the hfi distribution width of about 0.4 MHz should be largely associated with the dispersion of $T_\perp$. This results in a characteristic range of R_{GdH} values from about 3 to 3.2 Å. With the Gd−O distance of about 2.5 Å, this range of R_{GdH} could be explained, for example, by a variation of the angle between the H_2O ligand plane and Gd−O bond direction from 0° (Gd and all atoms of H_2O are in the same plane) to 55° (Gd and the hydrogens are located around the oxygen atom in the directions determined by its sp^3 hybrid orbitals). The range of variation of R_{GdH} due to possible structural variations is thus considerably greater than the error limits associated with the accuracy of determination of the central $T_\perp$ value.

Finally, we should note that although our assignment of the whole hfi distribution width to the anisotropic hfi constant seems very sensible, and the distribution width may be explained by moderate structural variations of the $Gd-OH_2$ fragment, one has to determine independently the spin densities on oxygens of water ligands in order to put this assignment on more solid ground.

4.5. Comparison with Earlier ENDOR Results. Comparing the hfi data for the Gd^{3+} aquo ion and Gd^{3+}HPDO3A we can see that they are identical within the accuracy limits of our measurements. The isotropic hfi constant in both cases is very close to zero and is much smaller than the maximal values of up to 0.45 MHz obtained previously in a single-crystal study.[24] In another single-crystal study,[23] however, the a_{iso} values obtained ranged from about −0.015 to about 0.04 MHz, very similar to those found in this work.

The anisotropic hfi constants in both cases correspond to the distance $R_{GdH} \approx 3.1$ Å that is in a good agreement with the distances estimated from single-crystal studies. On the other hand, as we already mentioned in the Introduction, the values of R_{GdH} found from a CW ENDOR study of Gd complexes in water/methanol glasses were in the range 2.5−3.1 Å.[21] A close look at that work shows that the problem was related to insufficient development of the ENDOR theory at that time. In particular, the components $3A_{1\perp}$ were interpreted by the authors as turning points of the proton transition lines belonging to $m_Z = \pm 1/2$ electron spin manifolds. A correct assignment of ENDOR spectral features recorded in ref 21 (that is, $A_{1\perp} \approx -2.64$ MHz and $A_{1||} \approx 5.79$ MHz) would lead for the Gd^{3+} aquo ion to $a_{iso} \approx 0.17$ MHz and $T_{1\perp} \approx -2.81$ MHz ($R_{GdH} \approx 3.05$ Å). One can see that the correct spectral assignment results in the hfi and R_{GdH} values for a glassy sample similar to those obtained for single crystals (although the hfi values for a glassy

sample are slightly overestimated because the experiments[21] were performed in the X-band).

5. Conclusion

In this work the proton ENDOR spectra of Gd^{3+} complexes in glassy solutions were studied theoretically and experimentally. In our analysis we were mostly concerned with the ENDOR spectra obtained while exciting the $+1/2 \leftrightarrow -1/2$ EPR transition because at moderately high mw frequencies and moderately low temperatures this transition provides the largest signal intensity (both EPR and ENDOR) and the best conditions for observing the ENDOR spectra.

Using numerical simulations we found that although the distortions of ENDOR spectra by the cfi can be quite considerable in a general case, the statistical distribution of the cfi parameters and relative orientations of the cfi and hfi axes in glassy samples results in ENDOR line shapes similar to the usual powder pattern determined by the hfi only, which greatly simplifies their analysis. The $A_\perp$ components in such cfi-averaged spectra are always easily observable and located at their correct positions, whereas the $A_{||}$ shoulders are somewhat broadened because of the effect of the cfi. Therefore, neglecting the cfi will generally result in some overestimation of hfi parameters found from the ENDOR spectra of glassy samples. The error of such estimates for Gd^{3+} complexes is, however, not very large even in the X-band, as we can deduce from comparison of the hfi parameters found in this work from the K_u-band spectra and with an account of the cfi ($a_{iso} = 0.03 \pm 0.02$ MHz, $T_\perp = -2.67 \pm 0.04$ MHz, and $R_{GdH} \approx 3.09 \pm 0.02$ Å for the Gd aquo complex) with those estimated without taking any account of the cfi from the X-band spectra recorded elsewhere[21] ($a_{iso} \approx 0.17$ MHz, $T_{1\perp} \approx -2.81$ MHz, and $R_{GdH} \approx 3.05$ Å).

We demonstrated that in 2D Mims ENDOR spectra obtained with appropriate dead time the effects of statically distributed cfi (typical for glassy samples) mostly disappear and the features corresponding to canonical orientations of hfi tensors are accentuated. In addition, in 2D Mims ENDOR spectra the lines from different electron spin manifolds are well separated, which greatly facilitates the interpretation of spectra from systems containing more than one type of proton. In principle, similar results could be obtained using HYEND[36] spectroscopy that offers a higher spectral resolution, but at the expense of lower sensitivity.

The numerical simulation of 1D and 2D Mims ENDOR spectra has allowed us to accurately determine the hfi parameters of water/methanol ligand protons for the Gd^{3+} aquo complex and Gd^{3+}HPDO3A MRI contrast agent. In both cases the isotropic hfi constant was close to zero (less than 0.1 MHz) and the anisotropic hfi constant was about -2.7 MHz, which corresponds to a Gd−H distance of about 3.1 Å. The accuracy of the anisotropic hfi constant measurement was better than ± 0.1 MHz, and thus the accuracy of distance determination was about ± 0.04 Å.

The Gd−H distance of 3.1 Å (or, with the distribution taken into account, from 3 to 3.2 Å) obtained in our experiments with glassy samples is thus similar to the distances obtained in earlier single-crystal studies. The accuracy of our hfi/distance measurements (without the hfi distribution) translates to a possible error of about $\pm 8\%$ in estimation of the distance factor $1/R^6_{GdH}$ entering the expressions for relaxivity of MRI contrast agents. This error is much smaller than the relaxivity variations for different complexes, and therefore $1/R^6_{GdH}$ can now be accurately accounted for in the assessment of various factors influencing the relaxivity.

Although in this work we were primarily interested in Gd^{3+} complexes, the theoretical results obtained here can be directly or with minor modifications applied to the analysis of ENDOR spectra of any other high-spin ion with weak cfi.

Acknowledgment. The authors acknowledge the NSF funding (DBI-9604939) for construction and modification of the pulsed EPR spectrometer used in this work.

References and Notes

(1) Caravan, P.; Ellison, J. J.; McMurry, T. J.; Lauffer, R. B. *Chem. Rev.* **1999**, *99*, 2293.
(2) Lauffer, R. B. *Chem. Rev.* **1987**, *87*, 901.
(3) Smirnova, T. I.; Smirnov, A. I.; Belford, R. L.; Clarkson, R. B. *J. Am. Chem. Soc.* **1998**, *120*, 5060.
(4) Kim, W. D.; Kiefer, G. E.; Maton, F.; McMillan, K.; Muller, R. N.; Sherry, A. D. *Inorg. Chem.* **1995**, *34*, 2233.
(5) Peters, J. A.; Huskens, J.; Raber, D. J. *Prog. Nucl. Magn. Reson. Spectrosc.* **1996**, *28*, 283.
(6) Micskei, K.; Helm, L.; Brucher, E.; Merbach, A. E. *Inorg. Chem.* **1993**, *32*, 3844.
(7) Powell, D. H.; Ni Dhubhghaill, O. M.; Pubanz, D.; Helm, L.; Lebedev, Y. S.; Schlaepfer, W.; Merbach, A. E. *J. Am. Chem. Soc.* **1996**, *118*, 9333.
(8) Toth, E.; Connac, F.; Helm, L.; Adzamli, K.; Merbach, A. E. *Eur. J. Inorg. Chem.* **1998**, 2017.
(9) Caravan, P.; Greenfield, M. T.; Li, X.; Sherry**,** A. D. *Inorg. Chem.* **2001**, *40*, 6580.
(10) *The Chemistry of Contrast Agents in Medical Magnetic Resonance Imaging*; Merbach, A. E., Toth, E., Eds.; Wiley: New York, 2001.
(11) Clarkson, R. B. In *Topics in Current Chemistry;* Krause, W., Ed.; Springer-Verlag: Berlin, **2002**; Vol. 221, p 202.
(12) Xu, J.; Franklin, S. J.; Whisenhunt, D. W. Jr.; Raymond, K. N. *J. Am. Chem. Soc.* **1995**, *117*, 7245.
(13) Smirnova, T. I.; Smirnov, A. I.; Belford, R. L.; Clarkson, R. B. *Magn. Reson. Mater. Phys., Biol. Med.* **1999**, *8*, 214.
(14) Caravan, P.; Cloutier, N. J.; Greenfield, M. T.; McDermid, S. A.; Dunham, S. U.; Bulte, J. W. M.; Amedio, J. C., Jr.; Looby, R. J.; Supkowski, R. M.; Horrocks, W. DeW., Jr.; McMurry, T. J.; Lauffer, R. B. *J. Am. Chem. Soc.* **2002**, *124*, 3152.
(15) Rast, S.; Borel, A.; Helm, L.; Belorizky, E.; Fries, P. H.; Merbach, A. E. *J. Am. Chem. Soc.* **2001**, *123*, 2637.
(16) Vander Elst, L.; Maton, F.; Laurent, S.; Seghi, F.; Chapelle, F.; Muller, R. N. *Magn. Reson. Med.* **1997**, *38*, 604.
(17) Muller, R. N.; Raduchel, B.; Laurent, S.; Platzek, J.; Pierart, C.; Mareski, P.; Vander Elst, L. *Eur. J. Inorg. Chem.* **1999**, 1949.
(18) Cohen, S. M.; Xu, J.; Radkov, E.; Raymond, K. N.; Botta, M.; Barge, A.; Aime, S. *Inorg. Chem.* **2000**, *39*, 5747.
(19) Churchill, M. R. *Inorg. Chem.* **1973**, *12*, 1213.
(20) Koenig, S. H.; Brown, R. D. *Prog. Nucl. Magn. Reson. Spectrosc.* **1990**, *22*, 487.
(21) Yim, M. B.; Makinen, M. W. *J. Magn. Res.* **1986**, *70*, 89.
(22) Clarkson, R. B.; Hwang, J. H.; Belford, R. L. *Magn. Reson. Med.* **1993**, *29*, 521.
(23) DeBeer, R.; Biesboef, F.; Van Ormondt, D. *Physica B* **1976**, *83*, 314.
(24) Fields, R. A.; Hutchison, C. A., Jr. *J. Chem. Phys.* **1985**, *82*, 1711.
(25) Astashkin, A. V.; Raitsimring, A. M. *J. Chem. Phys.* **2002**, *117*, 6121.
(26) Mims, W. B. *Proc. R. Soc. London, Ser. A* **1965**, *283*, 452.
(27) Liao, P. F.; Hartmann, S. R. *Phys. Rev. B* **1973**, *8*, 69.
(28) Astashkin, A. V.; Raitsimring, A. M.; Kennedy, A. R.; Shokhireva, T. Kh.; Walker, F. A. *J. Phys. Chem. A* **2002**, *106*, 74.
(29) Abragam, A.; Bleaney, B. *Electron Paramagnetic Resonance of Transition Metal Ions*; Clarendon Press: Oxford, U.K., 1970.
(30) Bennati, M.; Farrar, C. T.; Bryant, J. A.; Inati, S. J.; Weis, V.; Gerfen, G. J.; Riggs-Gelasco, P.; Stubbe, J.; Griffin, R. G. *J. Magn. Reson.* **1999**, *138*, 232.
(31) Arieli, D.; Vaughan, D. E. W.; Strohmaier, K. G.; Goldfarb, D. *J. Am. Chem. Soc.* **1999**, *121*, 6028.
(32) Goldfarb, D.; Strohmaier, K. G.; Vaughan, D. E. W.; Thomann, H.; Poluektov, O. G.; Schmidt, J. *J. Am. Chem. Soc.* **1996**, *118*, 4665.
(33) Brodbeck, C. M.; Iton, L. E. *J. Chem. Phys.* **1985**, *83*, 4285.
(34) Gaffney, B. J.; Yang, A. S. *Biophys. J.* **1987**, *51*, 55.
(35) Tan, X.; Bernardo, M.; Thomann, H.; Scholes, C. P. *J. Chem. Phys.* **1993**, *98*, 5147.

(36) Schweiger, A.; Jeschke, G. *Principles of Pulse Electron Paramagnetic Resonance*; Oxford University Press: New York, 2001.
(37) Doan, P.; Hoffman, B. *Chem. Phys. Lett.* **1997**, *269*, 208.
(38) Astashkin, A. V.; Kawamori, A. *J. Magn. Reson*. **1998**, *135*, 406.
(39) Ranon, U.; Hyde, J. *Phys. Rev.* **1966**, *141*, 259.
(40) Atherton, N. M.; Horsewill, A. J. *Mol. Phys.* **1979**, *37*, 1349.
(41) Getz, D.; Silver, B. L. *J. Chem. Phys.* **1974**, *61*, 630.
(42) Bryden, C. C.; Reilley, C. N.; Desreux, J. F. *Anal. Chem.* **1981**, *53*, 1418.